INTERNATIONAL JOURNAL FOR NUMERICAL METHODS IN FLUIDS
Int. J. Numer. Meth. Fluids 2009; **60**:669–689
Published online 9 September 2008 in Wiley InterScience (www.interscience.wiley.com). DOI: 10.1002/fld.1908

Experimental investigation of a maximum entropy assumption for acceleration terms within a poly-disperse moment framework

Stephen J. Scott and John S. Shrimpton*, †

Energy Technology Research Group, School of Engineering Sciences, University of Southampton, Southampton SO17 1BJ, U.K.

SUMMARY

Moment transport methods are being developed to model poly-dispersed multiphase flows by transporting statistical moments of the particle size–velocity joint probability density function (JPDF). A common feature of these methods is the requirement to reproduce or approximate the form of the JPDF from the transported moments for calculation of body force terms and other source terms. This paper examines the application of a maximum entropy technique against phase Doppler anemometry data sets from an electrostatically charged kerosene spray and also an automotive pressure swirl atomizer. An assessment of which moments are required to reproduce the JPDFs using a maximum entropy assumption to a sufficient level of accuracy is made. It is found that it is possible to reproduce the JPDFs to a high level of accuracy using a large number of moments; however, this incurs large computational overheads. If the moments to be transported are chosen on the basis of physical reasoning (such as the relationship between size and velocity due to drag) it is possible to reduce the number of moments to those which would be conserved via balance equations. This permits an approximation to the JPDF commensurate with the closure level of the moment transport method and thus the closure model method is naturally scalable with the degree of information from available conservation equations. Copyright © 2008 John Wiley & Sons, Ltd.

Received 25 March 2008; Revised 22 July 2008; Accepted 23 July 2008

KEY WORDS: maximum entropy; multiphase flow; closure method; drag force

INTRODUCTION

Dispersed multiphase flows are described by the transport of mass, momentum and energy in the form of particles dispersed within a gas or liquid carrier phase. Individual single component particles within a dispersed multiphase flow are characterized by their position, velocity, diameter and temperature at any point in time. In a typical industrial application (such as diesel injection in an internal combustion engine) the flow may consist of millions of particles, which interact

*Correspondence to: John S. Shrimpton, Energy Technology Research Group, School of Engineering Sciences, University of Southampton, Southampton SO17 1BJ, U.K.
†E-mail: john.shrimpton@soton.ac.uk

with each other and with the carrier phase. The high dimensionality and large range of scales induce complex phase transfer interactions and provide many challenges for engineers attempting to predict these flows computationally.

Microscopic methods attempt to model the full range of length and time scales present in the flow [1]. For the carrier phase this requires time and length scales resolved down to the Kolmorgorov scales. For the dispersed phase this requires adequate resolution of the gradients at the particle surface. Macroscopic methods involve only moments of the variables and hence much information needs to be reconstructed, ideally in a realizable manner, to provide conservation equations [2]. For a turbulent carrier phase a suitable model, such as the established eddy viscosity [3] (closure level of the Reynolds stresses) or second moment (closure at the triple correlations) methods, is required [4]. Mesoscopic methods attempt to capture the larger-scale features of the flow and model the smaller time and length scales, which consume the majority of the computational resources in these high-dimension problems. For the carrier phase large eddy simulation (LES) [5] is an example of a mesoscopic approach, similarly the point particle approximation [6] is a dispersed phase example.

In principle it is possible to resolve poly-dispersed two phase flows microscopically if appropriate boundary, initial and interface conditions are selected to completely describe the physical situation. If such an approach was adopted the carrier phase would be modelled using the Navier–Stokes equations and the discrete particle surfaces could be modelled as moving boundaries.

It is typical to make a continuum approximation for the carrier phase and to model the turbulence with either a mesoscopic (LES) or a macroscopic (RANS) assumption. For the discrete phase one can either directly approximate the particle population using a Lagrangian stochastic 'packet' approach [7] or use a continuum Eulerian approximation [8]. For the Lagrangian approach, whole particles are modelled as points, along with assumptions regarding mass momentum and energy exchange integrated over the particle surface. Employing a continuum approximation, in addition to the point particle assumption one must also define *phase* transport coefficients. Clearly the Lagrangian approach permits a direct approximation of the evolution of the particle population and in the present context is mesoscopic, whereas the Eulerian approach evolves moments of the particle population and is, in the present context, macroscopic.

While providing a direct approximation to the particle population, albeit at a point particle level, the Lagrangian approach is inherently time dependent and can be costly to account for all particle timescales. In addition, due to the stochastic nature of the Lagrangian particle modelling method it is necessary to obtain an ensemble of realizations in order to obtain statistically meaningful solutions. Finally it is difficult to accommodate dense particle regimes within this framework. Therefore, while the Lagrangian approach may seem an obvious approach to use to describe a particle population, there are some limitations and large computation times are usually required.

Until recently fully Eulerian methods for multiphase flow were dominated by the *two-fluid approach* [8, 9] in which a set of phase-averaged continuum equations representing conservation of mass, momentum and energy are derived. The equations were obtained by averaging the particle instantaneous equations over all realizations. This results in several closure issues that were normally resolved by appealing to empirical reasoning, once again established firstly for single-phase turbulence modelling [10].

In the case of poly-disperse dispersed particulate flows, the particle size distribution can be discretized into size 'bins' and Eulerian continuum equations can be written for each size class with appropriate exchange terms. Methods that do not bin the particle diameter dimension are relatively rare [11–19].

DOI: 10.1002/fld

Eulerian multiphase models based on stochastic Lagrangian methods [20] provide a firm mathematical basis for development. In this approach the continuum equations are derived from a transport equation for the probability density function (PDF) in particle phase space [21–24]. The principal advantage in this 'Lagrangian PDF approach' is that enables a rigorous transition from a stochastic mesoscopic description of individual particles within the flow, to an ensemble averaged macroscopic description of the particle phase as a whole. The approach guarantees that the family of equations, the size of which is governed by the closure level, are all internally consistent and the solution obtained from the equation family is realizable, providing any additional sources are also approximated consistently.

PHASE-SPACE DESCRIPTION

If a statistical description [24] is adopted for multiphase flows then the phase-space variables that characterize the flow are associated with a probability distribution functions (PDF) at any particular point in space and time. For example, the nth particle of the dispersed phase can be described in terms of particle velocity $U_i^{(n)}$, position $X_i^{(n)}$, and particle diameter $\Phi^{(n)}$ with corresponding phase space variables u_i, x_i, and ϕ. Ensemble averaging of this density function over all realizations results in the definition of the PDF. The Klimontovich fine grained phase-space density function at time t [25, 26] corresponding to these variables is then given as

$$f_p(u_i, \phi, x_i; t) = \sum_{n=1}^{N} \delta(x_i - X_i^{(n)}) \delta(u_i - U_i^{(n)}) \delta(\phi - \Phi^{(n)}) \tag{1}$$

Defining a particle volume fraction, α_p, may be combined to provide a mass density function defining within a phase-space volume of dimensions, $\mathrm{d}x_i\,\mathrm{d}\phi\,\mathrm{d}u_i$ centred on x_i, ϕ, and u_i:

$$F_p(u_i, \phi, x_i; t)\,\mathrm{d}x_i\,\mathrm{d}\phi\,\mathrm{d}u_i = \alpha_p(x_i; t) f_p(u_i, \phi, x_i; t)\,\mathrm{d}x_i\,\mathrm{d}\phi\,\mathrm{d}u_i \tag{2}$$

Using the definition of the PDF and the Lagrangian equations for the trajectories of the particle properties, it is possible to derive a transport equation for the particle PDF through phase space. This is analogous to the derivation of the Boltzmann equation from gas kinetic theory. Ignoring source terms for collisions, break up, the evolution of the FDF through phase space for a non-vaporizing/condensing liquid is defined as

$$\frac{\partial F}{\partial t} + \frac{\partial}{\partial x_i}(F u_i) + \frac{\partial}{\partial u_i}(F a_i) = 0 \tag{3}$$

From the PDF equation one can either compute the evolution of the PDF directly through phase space or derive transport equations for moments of the PDF, which represent measurable statistical quantities. For the phase-space variables, we have selected above, the first technique requires simulation in a seven-dimensional phase-space domain in addition to time.

We have chosen to follow the non-sectional route as proposed but not followed by Archambault [11] and to write conservation equations up to and including the triple correlations, which include the diameter as a variable. Table I lists the transported variables, and unclosed drift, coupling and moments higher than order three that require modelling. Clearly this set of equations constitutes a very large problem in both degrees of freedom and terms requiring closure. Indeed, if the complete model was to be implemented up to a second-order level of description plus the equation for $\langle \phi'_p \phi'_p \phi'_p \rangle$, this would require a numerical solution to 47 implicit transport equations

DOI: 10.1002/fld

Table I. Conserved variables and unclosed terms.

Variable	Drift	Coupling	Quartic
$\langle \alpha_f \rangle$			
$\langle \alpha_p \rangle$			
$\langle u_{f,i} \rangle$	$\langle A_{f,i} \rangle$	$S_{p\to f,i}^{\langle u_{f,i} \rangle}$	
$\langle \omega_f \rangle$	$\langle A_{f,i} \rangle$	$S_{p\to \Omega,i}^{\langle \omega_f \rangle}$	
$\langle u_{p,i} \rangle$	$\langle A_{p,i} \rangle$		
$\langle u_{s,i} \rangle$	$\langle A_{s,i} \rangle$	$S_{p\to s,i}^{\langle u_{s,i} \rangle}$	
$\langle \phi_p \rangle$	$\langle A_{p,i} \rangle$		
$\langle u'_{f,i} u'_{f,j} \rangle$	$\langle A_{f,i} u'_{f,j} \rangle$	$S_{p\to f,ij}^{\langle u'_{f,i} u'_{f,j} \rangle}$	
$\langle u'_{p,i} u'_{p,j} \rangle$	$\langle A_{p,i} u'_{p,j} \rangle$		
$\langle u'_{s,i} u'_{p,j} \rangle$	$\langle A_{s,i} u'_{p,j} \rangle, \langle A_{p,j} u'_{s,i} \rangle$	$S_{p\to s,ij}^{\langle u'_{f,i} u'_{p,j} \rangle}$	
$\langle \phi'_p u'_{p,i} \rangle$	$\langle A_{p,i} \phi'_p \rangle$		
$\langle u'_{s,i} u'_{s,j} \rangle$	$\langle A_{s,i} u'_{s,j} \rangle$	$S_{p\to s,ij}^{\langle u'_{s,i} u'_{s,j} \rangle}$	
$\langle \phi'_p u'_{s,i} \rangle$	$\langle A_{s,i} \phi'_p \rangle$	$S_{p\to s,i}^{\langle \phi'_p u'_{s,j} \rangle}$	
$\langle \phi'_p \phi'_p \rangle$			
$\langle u'_{f,i} u'_{f,j} u'_{f,k} \rangle$	$\langle A_{f,i} u'_{f,j} u'_{f,k} \rangle$	$S_{p\to f,ijk}^{\langle u'_{f,i} u'_{f,j} u'_{f,k} \rangle}$	$\langle u'_{f,i} u'_{f,j} u'_{f,k} u'_{f,m} \rangle$
$\langle u'_{p,i} u'_{p,j} u'_{p,k} \rangle$	$\langle A_{p,i} u'_{p,j} u'_{p,k} \rangle$		$\langle u'_{p,i} u'_{p,j} u'_{p,k} u'_{p,m} \rangle$
$\langle u'_{s,i} u'_{p,j} u'_{p,k} \rangle$	$\langle A_{s,i} u'_{p,j} u'_{p,k} \rangle \langle A_{p,i} u'_{s,j} u'_{p,k} \rangle$	$S_{p\to s,ijk}^{\langle u'_{s,i} u'_{p,j} u'_{p,k} \rangle}$	$\langle u'_{s,i} u'_{p,j} u'_{p,k} u'_{p,m} \rangle$
$\langle \phi'_p u'_{p,j} u'_{p,k} \rangle$	$\langle A_{p,i} \phi'_p u'_{p,j} \rangle$		$\langle \phi'_p u'_{p,j} u'_{p,k} u'_{p,m} \rangle$
$\langle u'_{s,i} u'_{s,j} u'_{p,k} \rangle$	$\langle A_{s,i} u'_{s,j} u'_{p,k} \rangle \langle A_{p,i} u'_{s,i} u'_{s,j} \rangle$	$S_{p\to s,ijk}^{\langle u'_{s,i} u'_{s,j} u'_{p,k} \rangle}$	$\langle u'_{s,i} u'_{s,j} u'_{p,k} u'_{p,m} \rangle$
$\langle \phi'_p u'_{s,j} u'_{p,k} \rangle$	$\langle A_{p,i} \phi'_p u'_{s,j} \rangle \langle A_{s,i} \phi'_p u'_{p,j} \rangle$	$S_{p\to s,ijk}^{\langle \phi'_p u'_{s,j} u'_{p,k} \rangle}$	$\langle \phi'_p u'_{s,j} u'_{p,i} u'_{p,j} \rangle$
$\langle \phi'_p \phi'_p u'_{p,k} \rangle$	$\langle A_{p,i} \phi'_p \phi'_p \rangle$		$\langle \phi'_p \phi'_p u'_{p,i} u'_{p,j} \rangle$
$\langle \phi'_p \phi'_p \phi'_p \rangle$			$\langle \phi'_p \phi'_p \phi'_p u'_{p,i} \rangle$

plus closures for the drift terms and third-order tensors. If the third-order terms are conserved this requires solution of 83 transport equations. If a monosize simulation is sought, our model simplifies to 34 equations and becomes identical to that proposed by Simonin [2]. There are therefore two clear advantages for following a non-sectional approach to solving multiphase flow problems with Eulerian equations. The first is that less transport equations are required. As noted above our non-sectional result of the Minier and Peirano derivation method [24] requires 83 equations, including third-order terms. By comparison, taking n size bins for n monosize particle 'phases' requires $7+32n$ equations where the third-order terms are modelled. This shows that even when n is rather small, say $n\sim 5$, the poly-disperse method is more efficient. The second advantage is that the proposed equation set is closed at the third-order level.

Of course, for every advantage gained a price must be paid. In the context of the proposed model the price is that the unclosed terms become significantly more complex because of the

DOI: 10.1002/fld

dependence of the particle timescale upon particle diameter. The complexity present is beyond the capability of a traditional empirical model, correlating a higher-order moment in terms of known, lower-order ones. What is required is a method to obtain the underlying PDF, based on a set of known constraints, moments in this case. Unknown moments are then obtained from integrating over this PDF.

The purpose of the present contribution is to propose a general method to approximate any source term within this model framework. In particular we focus on the acceleration due to drag that is realizable and consistent with the closure level of the equation family as a whole.

The acceleration term considered

The model derived in [27], based on [24], features unclosed terms relating to particle drag. For example, the transport equation for the particle Reynolds stresses, which features the correlation between particle aerodynamic drag A_p and fluctuating velocity u'_p:

$$\begin{aligned}\alpha_p\rho_p\frac{D_p}{Dt}[\langle u'_{p,i}u'_{p,j}\rangle] = &-\frac{\partial}{\partial x_k}[\alpha_p\rho_p\langle u'_{p,i}u'_{p,j}u'_{p,k}\rangle]\\ &-\alpha_p\rho_p\langle u'_{p,i}u'_{p,k}\rangle\frac{\partial\langle u'_{p,j}\rangle}{\partial x_k}-\alpha_p\rho_p\langle u'_{p,j}u'_{p,k}\rangle\frac{\partial\langle u'_{p,i}\rangle}{\partial x_k}\\ &+\alpha_p\rho_p\langle A_{p,i}u'_{p,j}+A_{p,j}u'_{p,i}\rangle \end{aligned} \tag{4}$$

Assuming Stokes drag for a monodisperse population and constant properties, this term can be expanded as

$$\langle A_{p,i}u'_{p,j}\rangle=\frac{1}{\tau}\langle(u'_{s,i}-u_{p,i})u_{p,j}\rangle=\frac{18\mu_f}{\rho_p\phi^2}\langle(u'_{s,i}-u_{p,i})u_{p,j}\rangle \tag{5}$$

where τ is a function of particle diameter ϕ and $u_{s,j}$ is the fluid velocity seen by the particle. For a monodisperse particle population, the unclosed term is a function of velocity correlations only. If a poly-disperse description is the objective, again assuming Stokes drag, the unclosed term now becomes

$$\langle A_{p,i}u'_{p,j}\rangle=\left\langle\frac{(u'_{s,i}-u_{p,i})u_{p,j}}{\tau}\right\rangle=\frac{18\mu_f}{\rho_p}\left\langle\frac{(u'_{s,i}-u_{p,i})u_{p,j}}{\phi^2}\right\rangle \tag{6}$$

and we now require mixed correlations of diameter, sampled fluid velocity and particle velocity. As demonstrated for Stokes drag, these correlations involve simple integer exponents of the phase-space variables. Unfortunately if a non-linear drag law (valid for $Re_p>1$) is adopted [28], the unclosed term then becomes a function of non-integer correlations, where C is the relative speed between fluid and particle:

$$\begin{aligned}\langle A_{p,i}u'_{p,j}\rangle &=\left\langle\left(1+\frac{Re^{2/3}}{6}\right)\frac{(u'_{s,i}-u_{p,i})u_{p,j}}{\tau}\right\rangle\\ &=\frac{18\mu_f}{\rho_p}\left\langle\frac{(u'_{s,i}-u_{p,i})u_{p,j}}{\phi^2}\right\rangle+\frac{3\mu_f^{1/3}\rho_f^{2/3}}{\rho_d}\left\langle\frac{(u'_{s,i}-u_{p,i})u_{p,j}C^{2/3}}{\phi^{4/3}}\right\rangle\end{aligned} \tag{7}$$

DOI: 10.1002/fld

The above problem highlights one example of the closure problem posed by macroscopic transport methods for the discrete phase where the particle diameter is not binned. In addition to this momentum source term, other momentum source terms may exist such those due to lift, rotation, acceleration, added mass, electrical forces and also terms representing mass and energy phase transfer. Some if not all of these physical mechanisms are empirically modelled, and many require non-linear, non-integer moments of several phase-space variables, some of which will not be available in conserved form via balance equations. Therefore, this issue is the norm rather than the exception and this present contribution offers an assessment of a general method to accommodate this problem.

CONSIDERATION OF A GENERAL CLOSURE METHOD

One option is to approximate unknown moments with combinations of known conserved ones, for instance, approximating $\langle \varphi^{1/2} \rangle$ as $\langle \varphi \rangle^{1/2}$. This method is not realizable locally or globally and is not considered further. Another option [14] is to use an assumed joint probability density function (JPDF). The method has the advantage that all moments are known analytically and is locally realizable. However, this method has a global realizability issue, in that an assumed PDF that may be valid at one location in space and time may possibly evolve into a form that violates the assumption of the PDF at another location. An assumed PDF also is not general in the sense that if the particle state vector enlarges or contracts on a problem-by-problem basis then the assumed PDF should also increase or decrease in dimension. This is generally not possible with the assumed PDF assumption, and therefore attention turns to PDF *reconstruction* methods.

One option is direct reconstruction [29]; however, extending this method to an arbitrary number of dimensions would be difficult. Therefore, the method cannot be considered general. Numerous different approaches have been adopted for various non-equilibrium stochastic systems and these methods can be classified as either linear or non-linear (a comprehensive discussion can be found in [30, 31]). Generally, equilibrium distributions are associated with a Maxwellian PDF, whereas non-equilibrium distributions are associated with PDFs with more complex forms. Linear representations of the non-equilibrium distribution correspond to a series expansion about the equilibrium distribution. Probably the most well-known closure of this type is the Chapman–Enskog expansion [32]. An alternative to the Chapman–Enskog expansion is Grad's representation [33]. Grad proposed an expansion to the equilibrium velocity distribution using multi-dimensional Hermite polynomials. Grad performed the expansion to third-order moments to obtain the well-known '13 moment expansion'. The fluid dynamics and to a large extent the RANS turbulence modelling community have proven the usefulness of the near-equilibrium approach. However, the fluid continuum and the turbulence fields can both rely to a large extent on a continuum hypothesis and that the 'equilibrium' conditions will restore if the driving force is removed. A poly-disperse phase cannot reliably follow this analogy due to the wide range of timescales present.

We now turn our attention to the non-linear representations for a non-equilibrium distribution. Probably the simplest of non-linear representations is the joint normal PDF, which does not conform to spherical symmetry (in contrast to the Maxwellian). The joint normal distribution suffers from the drawback that all odd-order moments are identically zero. The consequences of this limitation is that the joint normal PDF cannot represent non-equilibrium phenomena (such as heat flux) associated with odd-order moments. An alternative approach to generating a non-linear representation is based on the second characteristic function of the PDF [31]. This method is

DOI: 10.1002/fld

capable of generating distributions with non-zero odd-order moments; however, the method does not guarantee a realizable PDF in the sense that negative probabilities are possible. In addition to these methods several specialized techniques have been developed for specific physical phenomena (e.g. normal shocks [34]).

The non-linear method of interest here is that first utilized by Koopman [35], based on the concept of information entropy. This technique, known as the maximum entropy method (MEM), will be outlined in more detail in the following section, but it is essentially based on the concept of minimizing statistical bias of a JPDF. A JPDF is generated that satisfies a set of input constraints but makes no further assumption as to the form of the JPDF—the information entropy is maximized. The MEM (Koopman) method is attractive for several reasons: (i) sound conceptual foundations [36]; (ii) interdependence between even- and odd-order moments; and (iii) non-negative probabilities.

In summary the linear methods, while simpler in terms of algebraic complexity, are less likely to produce PDF representations capable of capturing non-equilibrium physics. In addition, these methods do not guarantee the absence of negative probabilities and hence do not satisfy realizability. Conversely, non-linear methods suffer from increased algebraic complexity but guarantee realizable distributions for larger deviations from equilibrium.

THE MAXIMUM ENTROPY METHOD

In 1948 Shannon [37] proposed the concept of information entropy for a discrete probability distribution. The entropy is defined for a group of M mutually exclusive events, each with probability p_m. Shannon's measure of the entropy or uncertainty of the discrete distribution is

$$H = -C \sum_{m=1}^{M} p_m \ln p_m \tag{8}$$

where C is an arbitrary positive constant. For a set of distribution moments, it is well known that an infinite set of JPDFs exist, which satisfy the moments. The MEM assumes that for a finite set of moments (constraints) the best estimate (least biased best guess) of the true JPDF is the one that maximizes the statistical entropy.

Given a continuous distribution in one dimension $f(x)$, the entropy of the distribution can be defined as the functional

$$H[f(x)] = -\int_{-\infty}^{+\infty} f(x) \ln[f(x)]\,\mathrm{d}x \tag{9}$$

and the distribution conforms to the normalization condition

$$J_0[f(x)] = \int_{-\infty}^{+\infty} f(x)\,\mathrm{d}x = 1 \tag{10}$$

and is subject to additional n constraints defined as

$$J_n[f(x)] = \int_{-\infty}^{+\infty} g_n(x) f(x)\,\mathrm{d}x = \langle g_n(x) \rangle \tag{11}$$

DOI: 10.1002/fld

The MEM objective is to maximize Equation (9) subject to the constraints prescribed by (10) and (11). Formulating the problem as an Euler–Lagrange equation, we have [38]

$$\left\{\frac{\partial}{\partial f}-\frac{\mathrm{d}}{\mathrm{d}x}\frac{\partial}{\partial f'}\right\}\left[-f\ln[f]+\lambda_0 f+\sum_{n=1}^{N}\lambda_n g_n(x)f\right]=0 \tag{12}$$

where $f'=\mathrm{d}f/\mathrm{d}x$ and the Lagrange parameters are denoted λ_n. The terms inside the square brackets are not functions of $f'(x)$; hence, the equation is simplified to

$$-\ln[f]-1+\lambda_0+\sum_{n=1}^{N}\lambda_n g_n(x)=0 \tag{13}$$

and by absorbing the constant (-1) into the parameter λ_0 this becomes

$$f(x)=\exp\left[\lambda_0+\sum_{n=1}^{N}\lambda_n g_n(x)\right] \tag{14}$$

From Equation (14) it is obvious that for real λ_n and $g_n(x)$, the PDF $f(x)$ will be non-negative and the realizability requirements are satisfied. Equation (14) demonstrates that the PDF is completely specified by the parameters λ_0 and λ_n, which in turn are associated with each of the constraints $\langle g_n(x)\rangle$. Equations (10), (11), and (14) form a closed but strongly non-linear set of equations. Ideally it would be possible to find analytical solutions of the form $\lambda_0=\lambda_n[\langle g_n(x)\rangle]$ and this has been the objective of recent research for near-equilibrium PDFs [30, 31]. In the situation under investigation here, we are interested in PDFs far from equilibrium; hence, a numerical solution is sought.

NUMERICAL METHOD

The solution of maximum entropy problem can be achieved using the method of Lagrange multipliers; however, this direct calculation requires the solution of a set of implicit non-linear equations. For problems of several phase-space dimensions with multiple constraints, solutions can be difficult to achieve and computationally expensive. An alternative to this method is to formulate a variational solution using the Lagrange multipliers as variational parameters according to the method of Alhassid *et al*. [39, 40]. This method requires formulation of a single-valued function F, defined by a phase domain and constraints, which itself is a function of the Lagrange parameters. The entropy constraints are expressed in discrete form according to

$$\sum_{m=1}^{M} g_n(x_m)\,p(x_m)=\langle g_n\rangle \tag{15}$$

where N is the number of constraints and the summation is made over all M discrete positions in the PDF phase space. Following the method of Alhassid *et al*. [39, 40] a single-valued function of the Lagrange parameters is derived:

$$F=\ln\sum_{n=1}^{N}\exp\left(\sum_{m=1}^{M}-\lambda_n B_{m,n}\right) \tag{16}$$

DOI: 10.1002/fld

where

$$B_{m,n} = g_n(x_m) - \langle g_n \rangle \tag{17}$$

and to achieve maximum entropy this function must be minimized by varying λ_n. Once obtained, the calculated values of λ_n are used to generate the MEM PDF using

$$p_m = \exp\left(-\lambda_0 - \sum_{n=1}^{N} \lambda_n g_n(x_m)\right) \tag{18}$$

Computational speed was not of interest in this preliminary investigation; hence, for convenience the MEM was coded using MATLAB. Minimization was achieved using the Nelder–Mead algorithm, which requires only function evaluations. The simplex algorithm attempts to enclose the function minimum inside a simplex (n-dimensional convex volume defined by $n+1$ linearly independent points). The algorithm requires an initial guess for the simplex points (Lagrange parameters) and then uses an iterative procedure of reflections, expansions and contractions to reduce the size of the simplex until it is small enough to enclose the minimum with the desired accuracy. Although alternative faster solution methods are available (e.g. conjugate gradient methods), the simplex method was selected for the MEM code because it is robust for large-dimensional problems and is suitable for non-smooth functions where the derivatives cannot be found.

Phase-space resolution

The MEM code was tested by generating a multi-dimensional PDF using a Gaussian random number generator, then taking the moments of this distribution, and using them as constraints in the MEM code and comparing the results. Good correlation between distributions was achieved although the peak value of the PDF was found to be sensitive to the phase-space discretization. This issue needed to be quantified because we compared a PDF generated from the MEM solver, where phase space was discretized using a uniform orthogonal Cartesian mesh, with an experimental PDF is generated by binning discrete data.

This issue is demonstrated in Figure 1 that illustrates PDFs for a randomly generated multivariate Gaussian data set of 10^4 points plotted using three different bin resolutions. Given that we know exactly how the marginal PDFs should look for a given set of constraints, Figure 1 can be used to determine an approximate number of data points per bin according to the ratio P/M_d^2 where P is the total number of points in the data set (10^4) and where M_d is the number of bins in each phase-space dimension. The first set of PDFs shows a low level of detail, whereas the last set resolves random fluctuations in the distribution caused by the limited sample size. For the case of this simple Gaussian distribution a value of $P/M_d^2 = 25$ (Figure 1(b)) was deemed appropriate and this value was used as a guide for use in plotting PDFs for the spray data sets due to their similarity with the Gaussian distribution. Figure 1 also illustrates the increase in PDF peak values as the bin size is reduced, which is an additional factor for consideration when comparing the MEM results with the original phase Doppler anemometry (PDA) data. This is shown in Figure 2, where the MEM solver is used to compute normal JPDF on increasing finely discretized phase-space domain. Figure 2(b) shows that the peak value, without interpolation, is sensitive to position of the peak value relative to the mesh points and produces sensible peak values for $M_d \geqslant 10$ or more.

DOI: 10.1002/fld

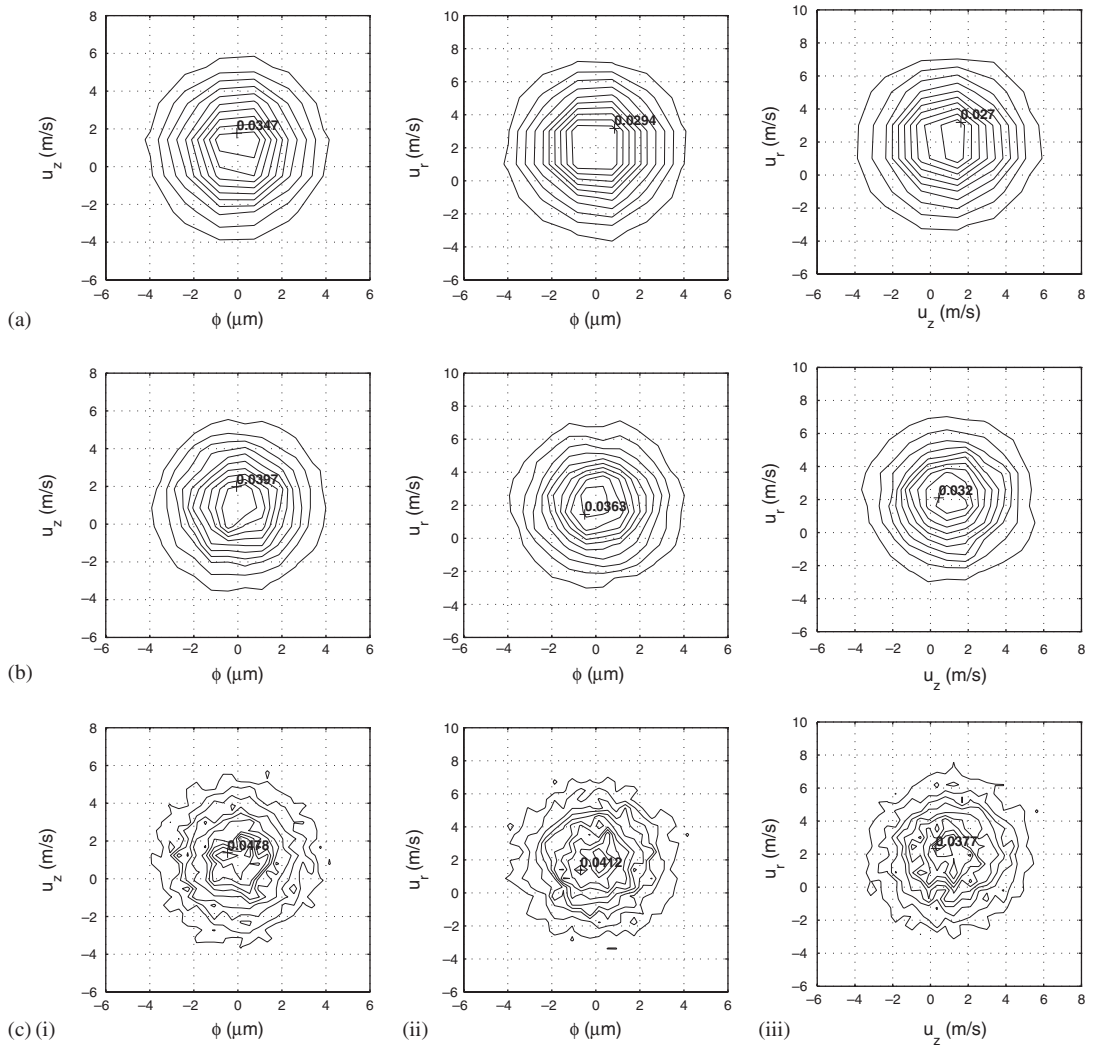

Figure 1. PDFs of (i) droplet size and axial velocity, (ii) droplet size and radial velocity and (ii) axial velocity and radial velocity generated using random Gaussian number generator $\mu_\phi = 0$, $\mu_u = 1$, $\mu_v = 2$, $\mu_\phi'^2 = 3$, $\mu_u'^2 = 4$, $\mu_v'^2 = 5$. Plotted for (a) $P/M_d^2 = 100$, (b) $P/M_d^2 = 25$, and (c) $P/M_d^2 = 6.25$.

EXPERIMENTAL DATA

Two sprays are considered in this paper and are shown in Figures 3 and 4. The first spray is a transient spray produced using a pressure swirl atomizer [41] for use in direct ignition spark ignition (DISI) engines and is shown in Figure 3. The second spray was a steady-state electrostatically charged kerosene spray [42] and is shown in Figure 4. The spray data sets were obtained using

DOI: 10.1002/fld

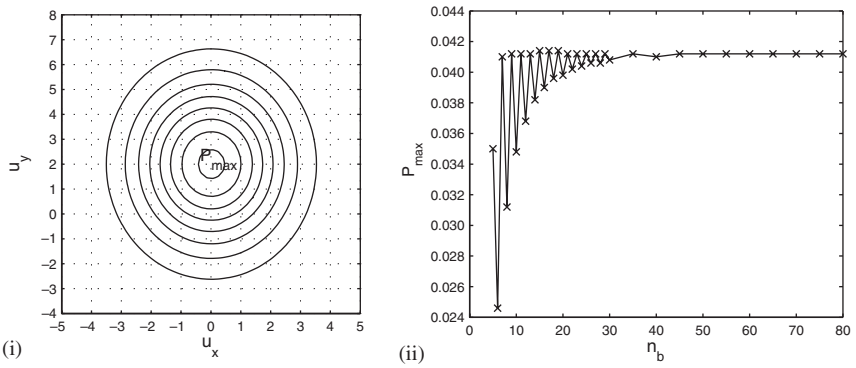

Figure 2. Variation of PDF peak with MEM bin resolution for a Gaussian input.

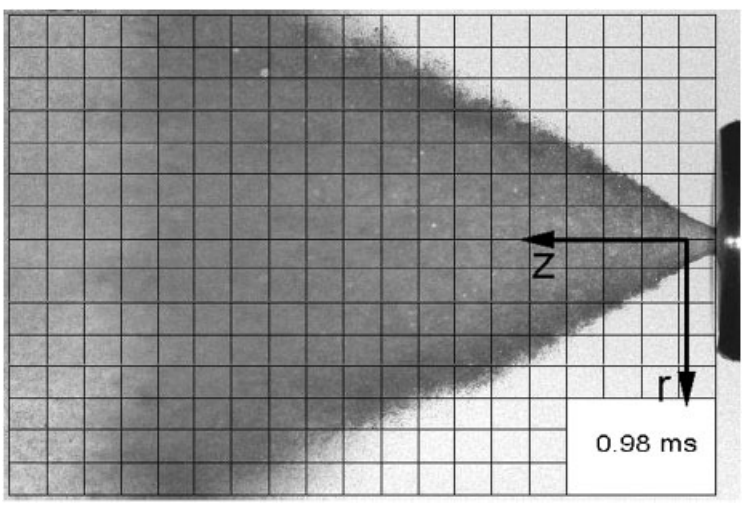

Figure 3. Photographic image of DISI pressure swirl spray.

the PDA method, measuring droplet size ϕ and two components of droplet velocity (axial u_z and radial u_r) simultaneously.

The first spray was generated using a DISI pressure swirl injector spraying at 50 bar gasoline pressure into air under atmospheric conditions for a relatively long injection event of 5 ms. For the purposes of this investigation it was necessary to obtain pseudo-steady data from the transient history of the spray PDF at the positions chosen. To achieve this, transient data were processed into time bins of duration 0.1 ms to identify a pseudo-steady region as shown in Figure 5. PDA data points outside this pseudo-steady region were discarded ($t<2$ ms, $t>5$ ms). This leads to a 45% reduction in the data set size, but cleaned up the shape of the raw PDF considerably, as evidenced by Figure 6. In addition to this the variance within each bin was calculated and checked for steady properties within this time interval.

For both data sets it was assumed that the velocity of the fluid at the particle position was zero; therefore, particle relative and actual velocities are equivalent. This is a simplification and

DOI: 10.1002/fld

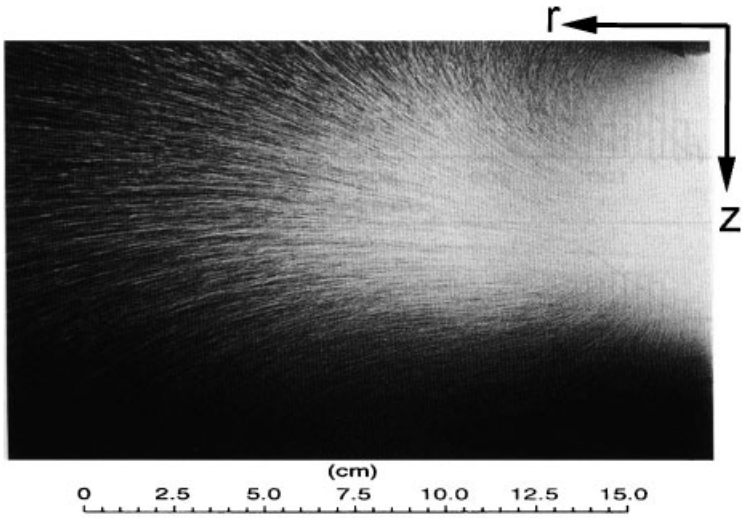

Figure 4. Photographic image of electrostatic kerosene spray.

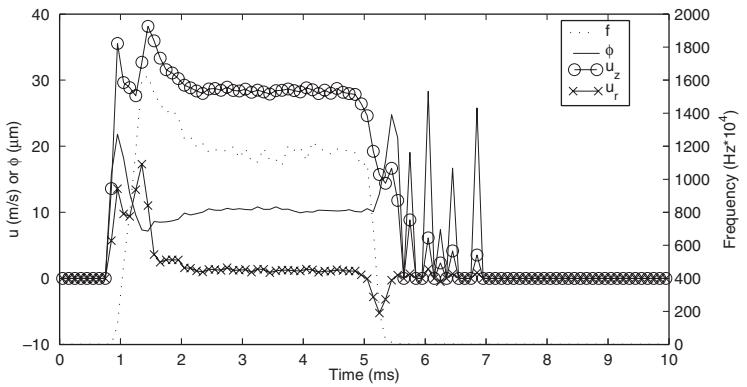

Figure 5. PDA sample rate f and mean quantities for DISI pressure swirl spray position PDA1A ($z=20\,\text{mm}, r=0\,\text{mm}$). PDA data sorted using 0.1 ms bin size.

while the particle dispersion due to the fluid turbulence, the present of the turbulence in the fluid is absent. An alternative approach to obtaining the carrier fluid velocity would be to (a) assume 'smaller' particles are travelling at the local carrier fluid velocity and (b) interpolated in time to the particle arrival time. This method would only be possible for the DISI spray, since no particles in the charged spray follow the carrier fluid.

In total 12 PDA measurement points (six in each data set) were investigated. For brevity just three of the interesting test cases are presented here—two points in the transient DISI pressure swirl spray (PDA1A, PDA1F) and one point in the steady charged spray (PDA2A). The first position in the pressure swirl spray PDA1A is axially located at a distance $z=20\,\text{mm}$ from the injector. The second position in the pressure swirl spray PDA1F is also at an axial distance of $z=20\,\text{mm}$ in the spray at a radial distance of $r=7.5\,\text{mm}$, which corresponds to a position in the edge of the

DOI: 10.1002/fld

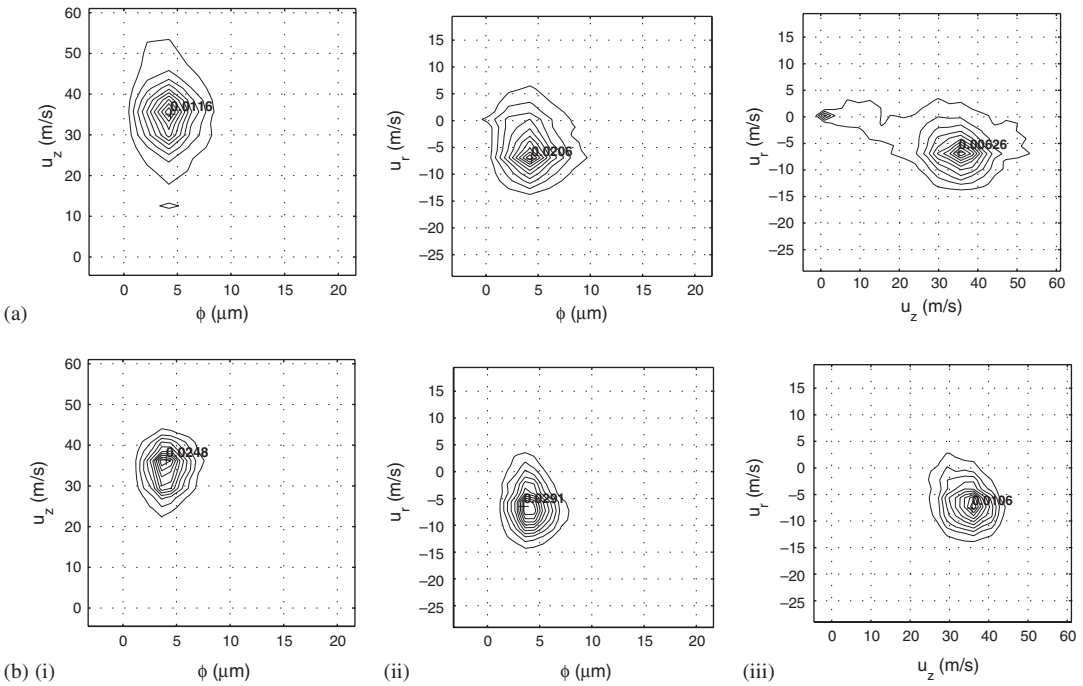

Figure 6. Unfiltered (a) and filtered (b) PDFs for the DISI pressure swirl spray position PDA1A ($z=20\,\text{mm}, r=0\,\text{mm}$). (i) Droplet size and axial velocity, (ii) droplet size and radial velocity and (iii) axial velocity and radial velocity. Plotted using 30×30 grid ($P/M_d^2=25$).

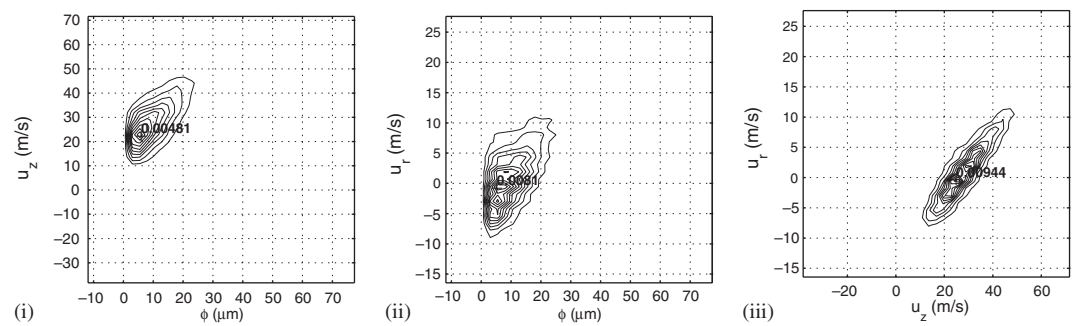

Figure 7. Filtered PDFs for the DISI pressure swirl spray position PDA1F ($z=20\,\text{mm}, r=7.5\,\text{mm}$). (i) Droplet size and axial velocity, (ii) droplet size and radial velocity and (iii) axial velocity and radial velocity. Plotted using 37×37 grid ($P/M_d^2=25$).

spray plume. Figure 7 shows the filtered PDFs for this position and in particular it highlights the correlation between axial and radial velocities. The second spray investigated is the steady charged hydrocarbon spray. The spray was produced using an atomizer with orifice diameter of 250 μm and a flow rate of 1.67 ml/s to give a mean injection velocity of 34 m/s ($Re=5100$ based on orifice

DOI: 10.1002/fld

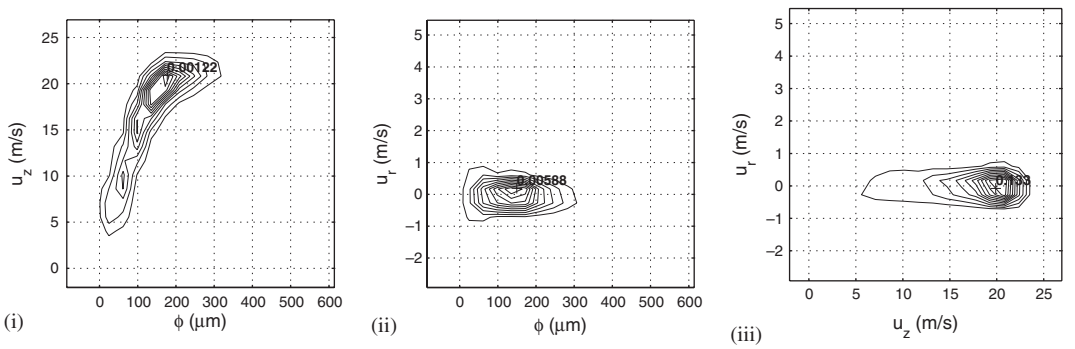

Figure 8. PDFs for the steady charged spray position PDA2A ($z=150\,\text{mm}, r=0\,\text{mm}$). (i) Droplet size and axial velocity, (ii) droplet size and radial velocity and (iii) axial velocity and radial velocity. Plotted using 20 × 20 grid ($P/M_d^2=25$).

diameter). The spray specific charge magnitude was $1.80\,\text{C/m}^3$. A single location in this spray is considered PDA2A at a position of $z=150\,\text{mm}$ and $r=0\,\text{mm}$. Figure 8 shows PDF contour plots for this position. Of particular interest is Figure 8(i) that shows the non-linear drag relationship between droplet size and axial velocity. The reason for the difference is the much larger range of diameters present in Figure 8 and the inertia these larger drops retain. Note that the charged spray data set was obtained under steady conditions; hence, no temporal filtering was required.

RESULTS: POSITION PDA1A

Figure 9 shows PDFs generated using MEM for position PDA1A in the DISI spray. The original PDA-based PDFs (Figure 6(b)) exhibit distributions that to all practical purposes are Gaussian in form. Comparison between the PDA and MEM PDFs would suggest that the PDFs can be reproduced reasonably well with just second-order central moment constraints (mean and variance of ϕ, u_z, u_r). Figure 9(b) shows MEM PDFs generated with the addition of third-order moment constraints and Figure 9(c) shows PDFs with the further addition of all covariances. These PDFs show minimal modification to the forms of the general shape PDFs, due to third-order and covariance moments being negligible and confirm the underlying PDF shape is Gaussian.

In general the MEM PDFs tend to underestimate the peak values of each PDF. This is the behaviour one may expect given that the MEM generates PDFs of least statistical bias. It is interesting to note that the peak values tend to increase as additional moments are added. In Figure 9(c) the peaks are approximately 5–12% higher than in Figure 9(a). A quantitative investigation of the discrepancy in peak values between MEM and PDA was attempted but due to the limited sample size for the PDA data it was difficult to isolate statistical noise from the PDF. Hence the magnitude and position of the PDA maximum is highly sensitive the mesh resolution.

RESULTS: POSITION PDA1F

Figure 10 shows MEM PDFs for the second point PDA1F in the DISI pressure swirl spray (edge of the spray cone). The PDA data (Figure 7) show correlation between all three variables

DOI: 10.1002/fld

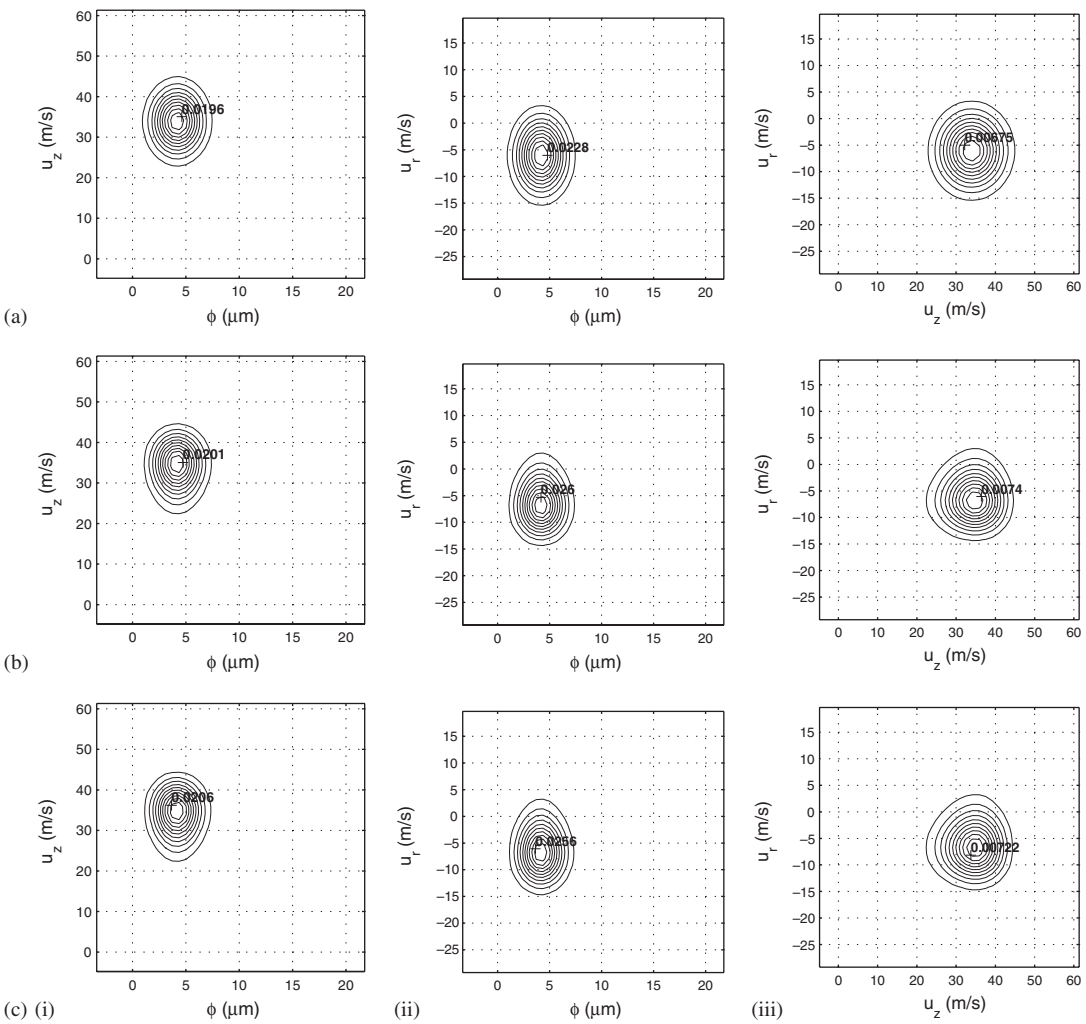

Figure 9. MEM generated PDFs for the DISI pressure swirl spray position PDA1A ($z=20\,\text{mm}, r=0\,\text{mm}$). (i) Droplet size and axial velocity, (ii) droplet size and radial velocity and (iii) axial velocity and radial velocity. Generated using moment constraints (a) to second order, (b) to third order, and (c) to third order with covariances.

(ϕ, u_z, u_r), most significantly between u_z and u_r. It is clear from Figure 11(a) that these PDFs cannot be accurately reproduced with only mean and variance constraints. If the MEM is further constrained by covariances $\langle \phi u_z \rangle, \langle \phi u_r \rangle$ and $\langle u_r u_z \rangle$, these correlations are reproduced as shown in Figure 10(b). Figure 10(c) shows the effect of further addition of third-order constraints but due to the symmetric nature of the original PDA data these constraints have negligible effect on the overall form of the MEM PDFs. Once again Figure 10 shows that as more constraints are added to the MEM solver, the peak PDF values increase towards the PDA peak values.

DOI: 10.1002/fld

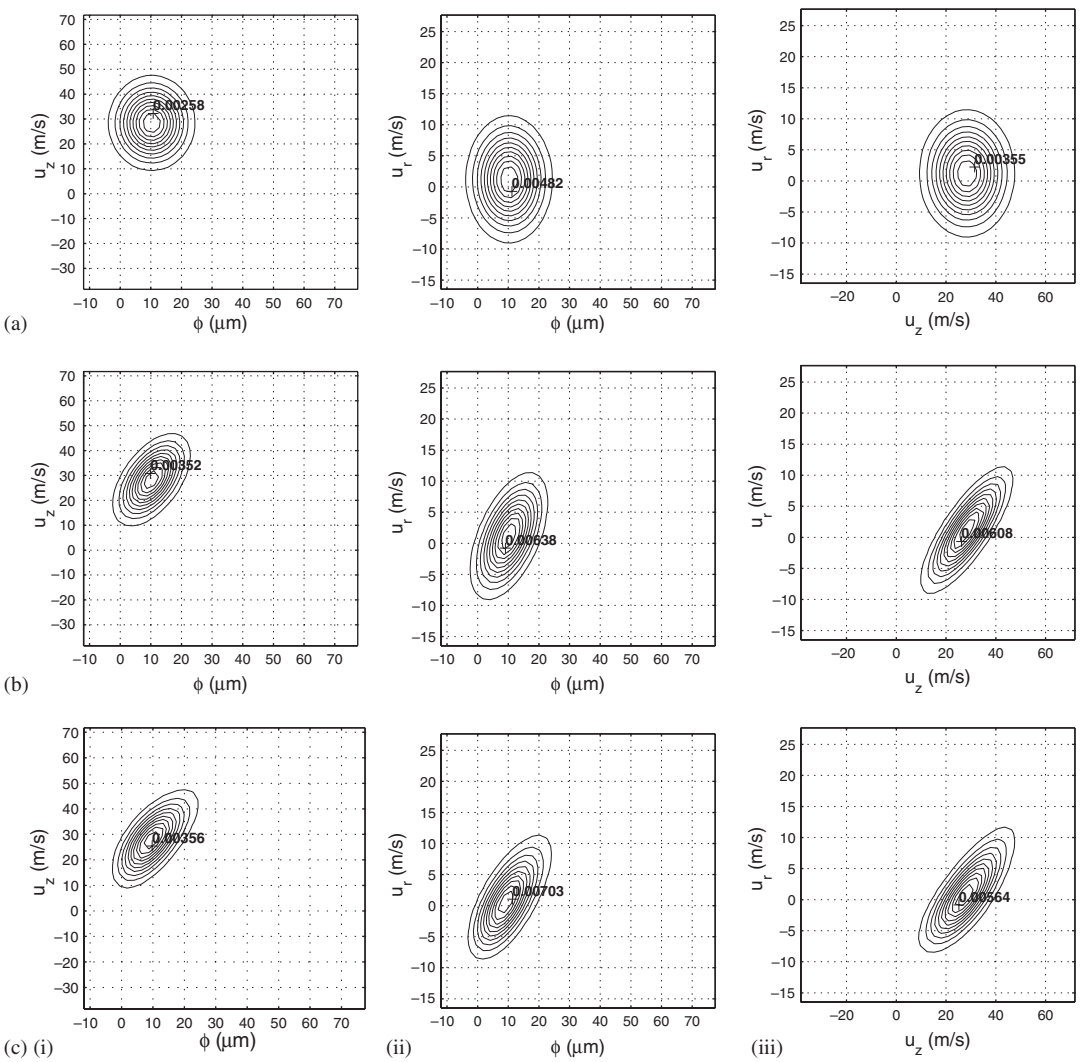

Figure 10. MEM generated PDFs for the DISI pressure swirl spray position PDA1F ($z = 20$ mm, $r = 7.5$ mm). (i) Droplet size and axial velocity, (ii) droplet size and radial velocity and (iii) axial velocity and radial velocity. Generated using moment constraints (a) to second order, (b) to second order with covariances, and (c) to third order with covariances.

RESULTS: POSITION PDA2A

Figure 11 shows MEM generated PDFs for the steady charged spray position PDA2A (Figure 8). It is clear from Figure 11(a) that means and variances alone are not sufficient to reproduce the form of the PDFs at this position. Using just these constraints the MEM fails to reproduce the cross correlations and asymmetry features present in Figure 8. The Gaussian-like PDFs are far too

DOI: 10.1002/fld

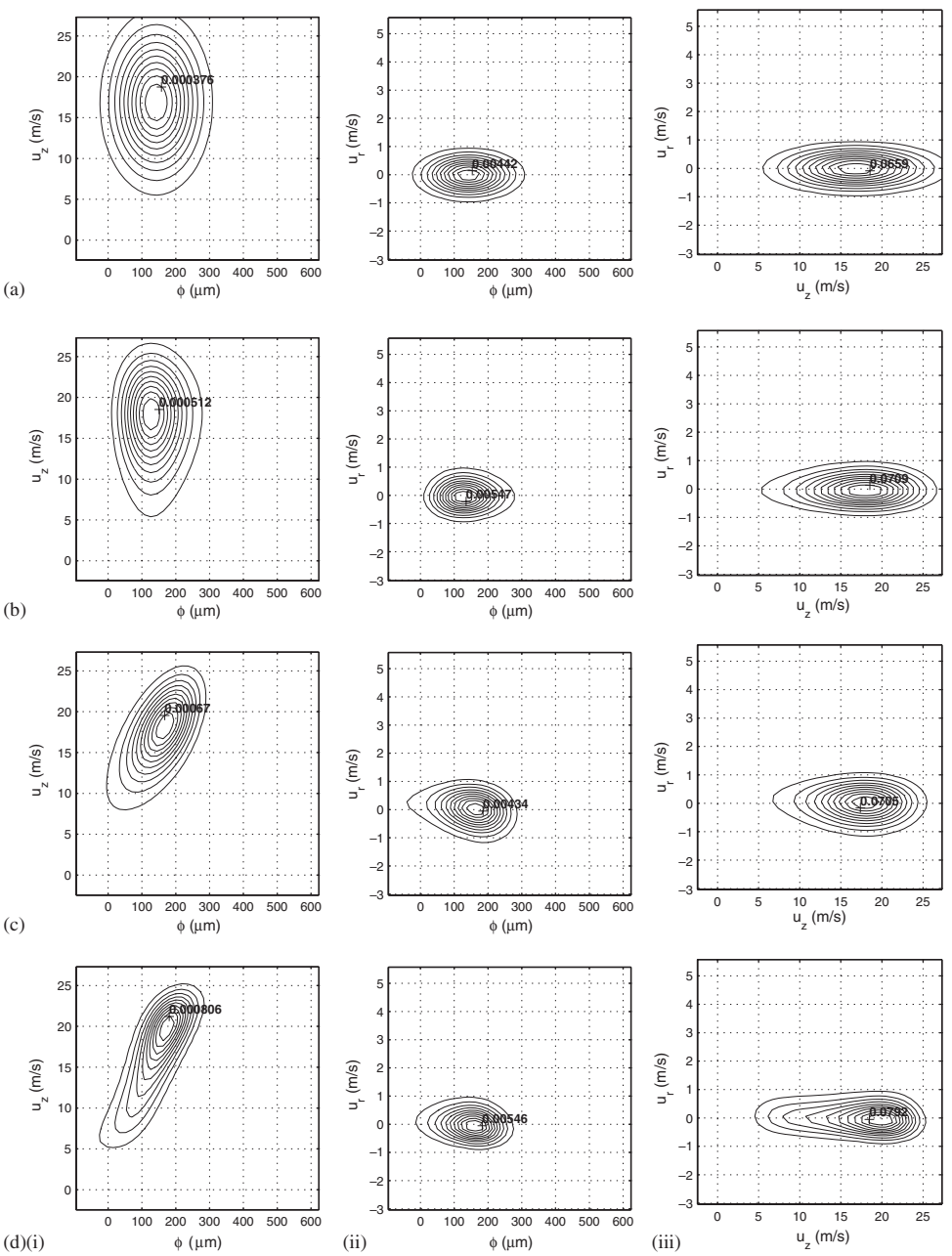

Figure 11. MEM generated PDFs for the steady charged spray PDA2A ($z = 20\,\text{mm}, r = 0\,\text{mm}$). (i) Droplet size and axial velocity, (ii) droplet size and radial velocity and (iii) axial velocity and radial velocity. Generated using moment constraints (a) to second order, (b) to third order, (c) to third order with covariances, and (d) to fourth order with covariances.

DOI: 10.1002/fld

diffuse and peak values are an order of magnitude below those of the PDA PDFs. Addition of third-order constraints (Figure 11(b)) allows the MEM to reproduce the off-centre peaks; however, the PDFs still fail to represent the forms of the original PDA data. Further improvements are gained through the addition of covariance constraints, particularly for the $\phi - u_z$ PDF (Figure 11(ci)). Further improvements are obtained when the MEM is constrained by fourth-order moments as shown in Figure 11(d).

RESULTS: DISCUSSION

The measure of the error between the PDA and MEM distributions was calculated separately for each position by summing the square of the differences at each location in the domain as shown in the following equation:

$$\varepsilon = \frac{1}{M_b^2} \sum_{m=1} (p_m^{\mathrm{PDA}} - p_m^{\mathrm{MEF}})^2 \tag{19}$$

where n is the number of 'bins' along each axis and hence M_b^2 points exist in the domain for each JPDF. Figure 12 shows the error plotted as a function of the central moment order for the two positions in the spray PDA1A and PDA1F.

Figure 12 shows a large reduction in the error when increasing the constraint order from one to two. This is to be expected because this effectively changes the MEM distribution from and exponential to Gaussian approximation to the 'real' PDA distribution. The trend as higher-order moments are added is a reduction in the error. There are exceptions to this trend where the addition of higher-order moments increases the error. This may due to the increased rigidity of the MEM solution as additional moments are added. The MEM code attempts to find the distribution of maximum entropy for a given set of constraints, and this is not necessarily the distribution that most accurately reproduces the PDA data. Figure 12 also shows the effect of the adding cross moments $\langle \phi u_z \rangle$, $\langle \phi u_r \rangle$ and $\langle u_z u_r \rangle$. For low-order central moments the addition of these constraints can significantly reduce the error.

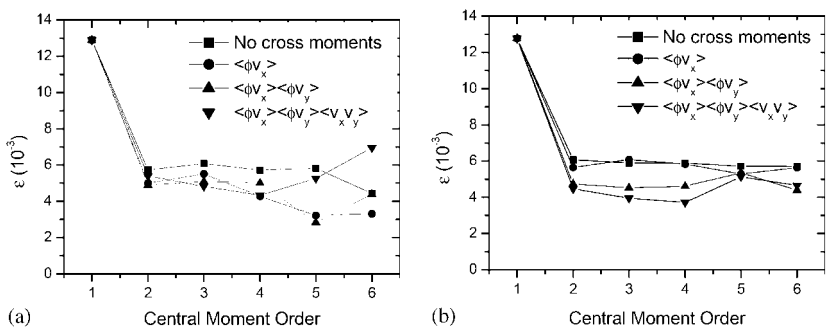

Figure 12. Measure of the error ε, between the PDA and MEF distributions for increasing order of central moments and with additional cross moments as indicated. (a) Position $z = 150\,\mathrm{mm}$, $r = 0\,\mathrm{mm}$ and (b) position $z = 120\,\mathrm{mm}$, $r = 40\,\mathrm{mm}$.

DOI: 10.1002/fld

CONCLUSIONS

The MEM has been proposed as a general closure method and evaluated for the specific case of the particle acceleration terms present in the moment model. In order to assess the suitability of the MEM experimental PDFs generated from two spray flows were compared with PDFs obtained from the MEM.

Obtaining the PDF of maximum entropy requires solution of a set of highly non- linear constraint equations. A numerical code has been developed, which is based on a Lagrange multipliers formulation of the maximum entropy problem. Solution requires minimization of a single-valued function of the Lagrange parameters and this is performed using a simplex minimization algorithm.

Comparisons between real PDFs obtained from experimental PDA data and MEM reconstructions show that the MEM method is capable of reasonable approximations of the multivariate PDFs given appropriate and sufficient constraints.

Essentially, the accuracy of the MEM method scales with the number and the order of the moment constraints. However, under certain conditions good estimates can be obtained with relatively few low-order constraints.

The MEM-based PDFs tend to underestimate the peak values and it is necessary to constrain the MEM further to enhance the accuracy of peak values. When considering the potential of the MEM in the context of a moment closure model for multiphase flow models, it must be realized that the suitability of the MEM is dependent on the nature of the flow. For simple isotropic flows a simple turbulent viscosity-type model for the particulate phase would provide sufficient information for constraint of the MEM and would allow the multiphase moment transport model to provide relatively accurate predictions relatively quickly. More complex flows exhibiting cross correlations and source terms that are not a function of transported moments require a more comprehensive set of constraints. Under these circumstances a model that transports second-order moments of the multiphase fluid would appear more suitable. However, where there is a large range of particle relaxation time scales, even a second-order moment transport model is likely to fail to capture all of the physics of the flow.

A quantitative assessment of the MEM proved difficult due to the limited sample size of the experimental data and the lack of fluid phase information. Hence, it was not possible to obtain a realistic MEM approximation to the $\langle A_{p,i} \rangle$ term present in the moment equations.

REFERENCES

1. Kajishima T, Takiguchi S. Interaction between particle clusters and particle-induced turbulence. *International Journal of Heat and Fluid Flow* 2002; **23**:639–646.
2. Simonin O. *Statistical and Continuum Modelling of Turbulent Reactive Particulate Flows Parts 1 and 2*. Von Karman Institute for Fluid Dynamics Lecture Series. Von Karman Institute: Rhode Saint Genèse (Belgium), 2000.
3. Jones WP, Launder BE. The prediction of laminarization with a two-equation model of turbulence. *International Journal of Heat and Mass Transfer* 1972; **15**:301–314.
4. Lauder BE, Reece GJ, Rodi W. Progress in the development of a Reynolds-stress turbulence closure. *Journal of Fluid Mechanics* 1975; **68**(3):537–566.
5. Sagaut P. *Large Eddy Simulation for Incompressible Flows*: *An Introduction* (3rd edn). Springer: Berlin, 2006. ISBN: 978-3-540-26344-9.
6. Crowe CT, Sommerfeld M, Tsuji Y. *Multiphase Flows with Droplets and Particles*. Elsevier: Amsterdam, 1997.
7. Dukowicz JK. A particle-fluid numerical model for liquid sprays. *Journal of Computational Physics* 1980; **35**: 229–253.

DOI: 10.1002/fld

8. Drew DA. Average field equations for two-phase media. *Studies in Applied Mathematics* 1971; **50**:133–166.
9. Drew DA. Mathematical modelling of two-phase flow. *Annual Review of Fluid Mechanics* 1983; **15**:261–291.
10. Rizk MA, Elghobashi SE. Two-equation turbulence model for dispersed dilute confined two-phase flows. *International Journal of Multiphase Flow* 1989; **15**:119–133.
11. Archambault MR. A maximum entropy moment closure approach to modelling the evolution of spray flows. *Ph.D. Thesis*, Stanford, 1999.
12. Archambault MR, Edwards CF, McCormack RW. Computation of spray dynamics by moment transport equations I: theory and development. *Atomization and Sprays* 2000; **13**:63–87.
13. Archambault MR, Edwards CF, McCormack RW. Computation of spray dynamics by moment transport equations II: application to quasi-one dimensional spray. *Atomization and Sprays* 2003; **13**:89–115.
14. Beck JC. Computational modelling of polydispersed sprays without segregation into droplet size classes. *Ph.D. Thesis*, UMIST, Manchester, U.K., 2000.
15. Beck JC, Watkins AP. The droplet number moments approach to spray modelling: the development of heat and mass transfer sub-models. *International Journal of Heat and Fluid Flow* 2003; **24**:242–259.
16. Beck J, Watkins AP. Simulation of water and other non-fuel sprays using a new spray model. *Atomization and Sprays* 2003; **13**:1–26.
17. White AJ, Hounslow MJ. Modelling droplet size distributions in polydispersed wet-steam flows. *International Journal of Heat and Mass Transfer* 2000; **43**:1873–1884.
18. Laurent F, Massot M. Multi-fluid modelling of laminar polydispersed spray flames: origin, assumptions and comparison of sectional and sampling methods. *Combustion Theory and Modelling* 2001; **5**:537–572.
19. Laurent F, Massot M, Villedieu P. Eulerian multi-fluid modelling for the numerical simulation of coalescence in polydisperse dense liquid sprays. *Journal of Computational Physics* 2004; **194**:505–543.
20. Pope SB. Lagrangian PDF methods for turbulent flows. *Annual Review of Fluid Mechanics* 1994; **26**:23–63.
21. Pandya RVR, Mashayek F. Probability density function modelling of evaporating droplets dispersed in isotropic turbulence. *AIAA Journal* 2001; **39**:1909–1915.
22. Reeks MW. On a kinetic equation for the transport of particles in turbulent flows. *Physics of Fluids A* 1991; **3**:446–456.
23. Zaichik LI. A statistical model of particle transport and heat transfer in turbulent shear flows. *Physics of Fluids* 1999; **11**:1521–1534.
24. Minier J-P, Peirano E. The PDF approach to turbulent polydispersed two-phase flows. *Physics Reports* 2001; **352**:1–214.
25. Subramaniam S. Statistical modelling of sprays using the droplet distribution function. *Physics of Fluids* 2001; **13**:624–642.
26. Subramaniam S. Statistical representation of a spray as a point process. *Physics of Fluids* 2000; **12**:2413–2431.
27. Scott SJ. A PDF based method for modelling polysized particle laden turbulent flows without size class discretisation. *Ph.D. Thesis*, Imperial College London, U.K., 2006.
28. Putnam A. Integratable form of droplet drag coefficient. *ARS Journal* 1961; **31**:1467–1468.
29. John V, Angelov I, Oncul AA, Thevenin D. Techniques for the reconstruction of a distribution from a finite number of its moments. *Chemical Engineering Science* 2007; **62**:2890–2904.
30. Volpe EV, Baganoff D. Maximum entropy PDFs and the moment problem under near-Gaussian conditions. *Probabilistic Engineering Mechanics* 2003; **18**:17–29.
31. Volpe EV. Closure relations as determined by the maximum entropy method and near equilibrium conditions. *Ph.D. Thesis*, Stanford, 2000.
32. Chapman S, Cowling MA. *The Mathematical Theory of Non-uniform Gases*. Cambridge University Press: Cambridge, 1960.
33. Grad H. On the kinetic theory of rarefied gases. *Communications on Pure and Applied Mathematics* 1949; **2**:331–407.
34. Nathenson M, Baganoff D. Constitutive relations based on the Mott-Smith distribution function. *Physics of Fluids* 1973; **16**:1232–1244.
35. Koopman BO. *Relaxed Motion in Irreversible Molecular Statistics*. Stochastic Processes in Chemical Physics, vol. 15, 1969; 37–63.
36. Paris J, Vencovska A. In defense of the maximum entropy inference process. *International Journal of Approximate Reasoning* 1997; **17**:77–103.
37. Shannon CE. A mathematical theory of communication. *Bell Systems Technical Journal* 1948; **27**:379–623.
38. Kreyszig E. *Advanced Engineering Mathematics*. Wiley: New York, 1999.

DOI: 10.1002/fld

39. Alhassid Y, Agmon N, Levine RD. An upper bound for the entropy and its applications to the maximal entropy problem. *Chemical Physics Letters* 1978; **53**:22–26.
40. Alhassid Y, Agmon N, Levine RD. An algorithm for finding the distribution of maximal entropy. *Journal of Computational Physics* 1979; **30**:250–258.
41. Wigley G. Presentation—some data with regard to imaging and PDA studies of the Mitsubishi GDI injector spraying at 50 bar gasoline pressure into air under atmospheric conditions, 2004.
42. Shrimpton JS, Yule AJ. Characterisation of charged hydrocarbon sprays for application in combustion systems. *Experiments in Fluids* 1999; **26**:460–469.

DOI: 10.1002/fld